Supplemental Material for "Thermally-driven electronic topological transition in FeTi"

F. C. Yang,[1] J. A. Muñoz,[1,2] O. Hellman,[1] L. Mauger,[1] M. S. Lucas,[1,3] S. J. Tracy,[1] M. B. Stone,[4] D. L. Abernathy,[4] Yuming Xiao,[5] and B. Fultz[1]

[1] *Applied Physics and Materials Science, California Institute of Technology, Pasadena, CA 91125*
[2] *The Datum Institute, Beaverton, OR 97005*
[3] *Air Force Research Laboratory, Wright-Patterson AFB, OH 45433*
[4] *Quantum Condensed Matter Division, Oak Ridge National Laboratory, Oak Ridge, TN 37831*
[5] *HPCAT, Geophysical Laboratory, Carnegie Institution of Washington, Argonne, IL, 60439*

(Dated: July 15, 2016)

PACS numbers: 63.20.Ry, 63.20.kd, 71.18.+y, 71.20.Lp, 63.20.dd

EXPERIMENTAL

Sample Preparation

The FeTi sample for neutron scattering measurements was synthesized by arc-melting 99.98% pure Ti and 99.97% pure Fe in the equiatomic ratio under an argon atmosphere. There was a negligible mass loss and no visible oxidation after melting. The brittle sample was crushed into a fine powder. Samples for x-ray measurements were synthesized in the same way, but were 96% enriched with ^{57}Fe. Conventional characterization was performed with x-ray diffractometry using Cu K_α radiation. All samples were found to have the $B2$ structure and no traces of other phases. These diffraction measurements included the determination of thermal expansion using a furnace for in situ measurements. The lattice parameters of $B2$ FeTi were determined to be 2.978 Å at 300 K; 2.984 Å at 523 K; 2.991 Å at 750 K. The coefficient of linear thermal expansion was 2.9×10^{-5}/K.

Scattering Measurements

Nuclear resonant inelastic x-ray scattering (NRIXS) measurements were performed at beamline 16 ID-D at the Advanced Photon Source at Argonne National Laboratory. NRIXS is sensitive only to the motions of ^{57}Fe atoms, so it provides partial phonon density of states (DOS) curves for Fe alone. For measurements at 300, 523, 748, and 1035 K, the sample was loosely dispersed between two Kapton polyimide films and then accommodated in a custom-built vacuum furnace. The sample was fixed at a grazing angle to the x-ray beam and an avalanche photodiode detector (APD) was set on top of the furnace at a right angle with the beam. The energy was scanned from −90 to +90 meV around 14.413 keV, the resonant energy of ^{57}Fe, in several scans that were combined for final analysis. The energy resolution of all NRIXS measurements was measured to be 2.2 meV (FWHM) at the elastic line. The NRIXS data were reduced using the PHOENIX code [1].

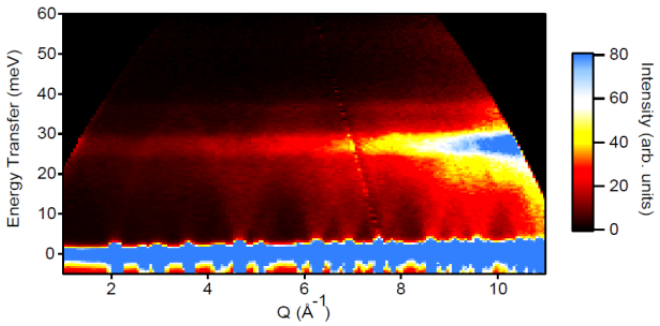

FIG. 1. Neutron scattering function $S(Q,E)$ spectrum of FeTi at 300 K.

Inelastic neutron scattering (INS) measurements were performed with the ARCS spectrometer [2] at the Spallation Neutron Source at Oak Ridge National Laboratory. The sample was loaded into an Al can which was then mounted in a low-background vacuum furnace for measurements at 300, 523, and 748 K. The nominal incident neutron energy was 80 meV. The energy resolution was 1.7 meV at an energy transfer of 40 meV, increasing to 3.1 meV at the elastic line (FWHM). The empty Al can was measured at all temperatures and subtracted from the measured spectra of the sample. The data reduction was performed using the DANSE software [3], giving the neutron-weighted DOS curves $g_{\rm NW}(\varepsilon)$ shown in Fig.2. Our NRIXS and INS spectra had very similar energy resolutions over much of the phonon spectra, and this permitted direct comparisons.

The neutron-weighting arises from the differences in the masses and neutron scattering cross-sections for each element and isotope. The neutron-weighted curves from INS could be corrected using the partial phonon DOS $g_{\rm Fe}(\varepsilon)$ obtained from NRIXS as described in Refs. [4–7]. Results are shown in the "neutron-weight-corrected DOS" panel in Fig. 2, noting that

$$g_{\rm NW}(\varepsilon) \simeq \frac{\sigma_{\rm Fe}}{M_{\rm Fe}} g_{\rm Fe}(\varepsilon) + \frac{\sigma_{\rm Ti}}{M_{\rm Ti}} g_{\rm Ti}(\varepsilon), \qquad (1)$$

where the ratios of the neutron cross section to molar

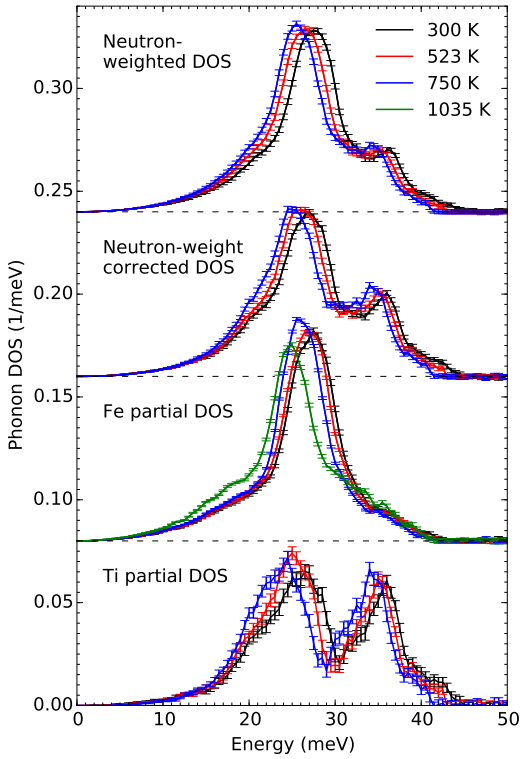

FIG. 2. Phonon DOS curves for FeTi at elevated temperatures. The neutron-weighted DOS curves were obtained from INS measurements and the Fe partial DOS curves from NRIXS measurements. The two data sets were combined to obtain neutron-weight-corrected DOS curves and Ti partial DOS curves. Error bars from counting statistics.

mass σ_d/M_d are 0.208 and 0.091 barns/amu for Fe and Ti, respectively. The partial Ti phonon DOS $g_{\mathrm{Ti}}(\varepsilon)$ was also obtained using this approach and is shown in the lower panel of Fig. 2.

COMPUTATIONAL DETAILS

Density Functional Theory

Density functional theory (DFT) calculations [8] were performed with VASP [9, 10] with projector augmented wave potentials with the Perdew-Burke-Ernzerhof (PBE) exchange-correlation functional [11] and an energy cutoff of 500 eV. The equilibrium volume of the structure was optimized to minimize the total energy. Spin-polarized calculations gave a negligible magnetic moment, in agreement with experimental results in Ref. [12].

The 0 K electronic band structure and Fermi surface were computed on the FeTi two-atom unit cell with a $80\times80\times80$ grid of k-points, sampled with the Monkhorst-Pack scheme [13]. The dense grid allowed for a greater sampling of phonon wavevectors which may span nesting features of the Fermi surface.

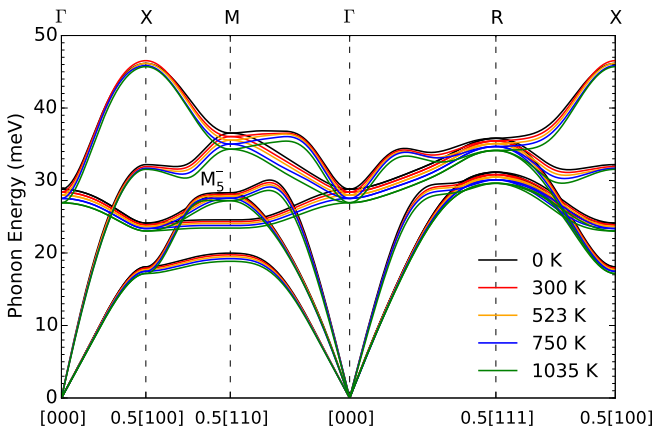

FIG. 3. FeTi phonon dispersions calculated in the quasiharmonic model.

To assess the effect of thermal expansion on the phonons in FeTi, phonon dispersions shown in Fig. 3 were calculated under the quasiharmonic approximation using the Parlinski-Li-Kawazoe method [14] implemented in the PHONOPY code [15]. The calculations were performed on 128-atom $4\times4\times4$ supercells with a $6\times6\times6$ k-point mesh and a grid of atom displacements of 0.01 Å for the temperatures 0, 300, 523, 750, and 1035 K. The volumes of the supercells were calculated by minimizing the free energy $F(T,V)$:

$$F(T,V) = E_0(V) + \int d\varepsilon\, g(\varepsilon)\left[\frac{\varepsilon}{2} + k_{\mathrm{B}}T\ln\left(1-e^{-\varepsilon/k_{\mathrm{B}}T}\right)\right]. \quad (2)$$

Ground-state energies $E_0(V)$ were calculated separately for each volume, and the DOS $g(\varepsilon)$ were calculated with lattice parameters that produced the minimized volume at each temperature. The calculated lattice parameters were smaller than the experimental ones by 0.7%. Figure 3 shows that the softening of the M_5^- phonon mode from thermal expansion alone is small compared to the large anomalous softening discussed in the main text.

Density Functional Perturbation Theory

Density functional perturbation theory calculations [16] were performed with Quantum ESPRESSO [17] with ultrasoft pseudopotentials [18] and the PBE exchange-correlation functional. The electron-phonon interaction matrix elements were first calculated on a $20\times20\times20$ k mesh and a $10\times10\times10$ q mesh, and later interpolated to a $60\times60\times60$ q mesh through Fourier interpolation implemented in the package. The matrix elements were then used to compute the electron-phonon linewidth plotted in Fig. 4. It is seen that EP linewidths of the longitudinal optical modes along the Γ-X, Γ-M, and Γ-R symmetry lines are large compared to the negligible linewidths of many other modes, such as the M_5^- mode.

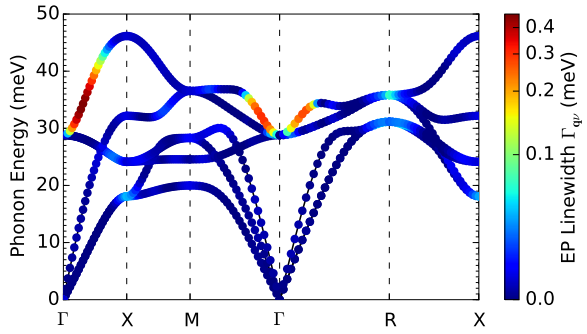

FIG. 4. Calculated 0 K electron-phonon linewidths displayed over the 0 K FeTi phonon dispersion.

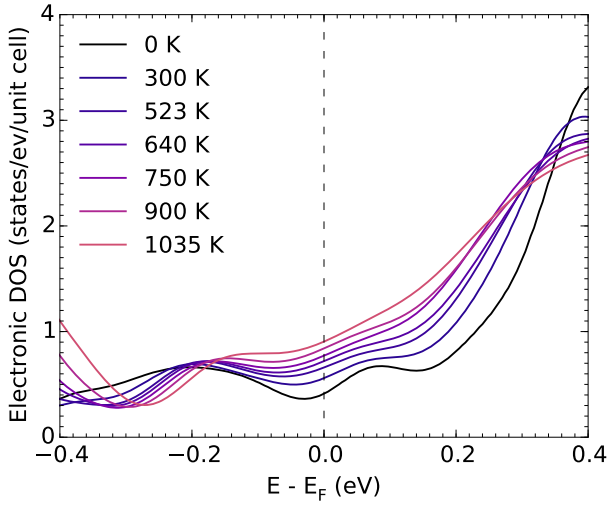

FIG. 5. Electronic DOS for FeTi from 0 to 1035 K. Obtained from AIMD and static DFT calculations.

Ab-Initio Molecular Dynamics

Ab-initio molecular dynamics (AIMD) calculations were performed using VASP with the potentials given in the DFT section on 128-atom supercells using a $2\times2\times2$ k-point mesh for 23 temperatures from 300 to 1500 K. The energy cutoff was 400 eV and the Monkhorst-Pack scheme was used to sample the Brillouin zone. Each simulation was carried out for over 10,000 timesteps using a canonical ensemble and the standard Nosé thermostat [19]. The electronic DOS curves shown in Fig. 5 were computed for each temperature from 0 to 1035 K by averaging the recomputed densities of states from 20 saved configurations using a $3\times3\times3$ k-point mesh. For each temperature, the BandUP code[20, 21] was performed on five of these configurations with 81 k-points along each high symmetry direction. The mean energies $\widetilde{\varepsilon}_{\mathbf{k}m}$ and smearing widths $\Delta\varepsilon_{\mathbf{k}m}$ of the bands were obtained from BandUP.

The temperature-dependent effective potential (TDEP) method [22, 23] was used primarily to calculate second-order force constants, which were then used to calculate the phonon dispersions and phonon DOS. For a few temperatures, the third-order force constants were also calculated from the model Hamiltonian fit to the potential energy surface at the most probable positions of atoms in an AIMD simulation:

$$\hat{H} = U_0 + \sum_i \frac{\mathbf{p}_i^2}{2m_i} + \frac{1}{2}\sum_{ij\alpha\beta}\phi_{ij}^{\alpha\beta}u_i^\alpha u_j^\beta + \frac{1}{3!}\sum_{ijk\alpha\beta\gamma}\psi_{ijk}^{\alpha\beta\gamma}u_i^\alpha u_j^\beta u_k^\gamma \quad (3)$$

where ϕ_{ij} and ψ_{ijk} are second- and third-order force constants, $\mathbf{p}$ is the momentum, and u_i^α is the Cartesian component α of the displacement of atom i. The third-order force constants account for cubic anharmonicity associated with phonon-phonon interactions [24]. The thermal phonon-phonon interaction shifts $\Delta(T)$ of a phonon mode $\mathbf{q}\nu$ calculated from the third-order force constants were negligible compared to the calculated phonon thermal softening induced by the adiabatic EPI. With this method, the effects of quartic anharmonicity are included by renormalizing the quadratic force constants.

Spanning Vectors

The histogram in Fig. 5 of the main text was obtained by counting spanning vectors from one of the new topological features around the R symmetry points to the rest of the Fermi surface. The vectors were counted in the Brillouin zone defined by an $80\times80\times80$ grid of k-points. For each spanning vector, the conservation of momentum and energy was required:

$$\widetilde{\varepsilon}_{\mathbf{k}+\mathbf{q}n} - \varepsilon_{\mathbf{k}m} \pm \hbar\omega_{\mathbf{q}\nu} - c_i\sigma \leq \Delta\varepsilon_{\mathbf{k}+\mathbf{q}n}, \quad (4)$$

where $\mathbf{k}+\mathbf{q}n$ is a state on one of the new topological features around the R symmetry points, $\mathbf{k}m$ is a state from the rest of the Fermi surface, $\widetilde{\varepsilon}_{\mathbf{k}+\mathbf{q}n}$ is the mean energy of the state $\mathbf{k}+\mathbf{q}n$ calculated by BandUP, $\varepsilon_{\mathbf{k}m}$ is equal to the Fermi energy, and $\hbar\omega_{\mathbf{q}\nu}$ is the energy of the phonon mode with polarization ν and wavevector $\mathbf{q}$. The smearing width $\Delta\varepsilon_{\mathbf{k}+\mathbf{q}n}$ describes the broadening of the electron pocket induced by the thermal disorder of the Fe and Ti atoms at higher temperatures.

The $c_i\sigma$ term describes the thermal excitation of electrons, where $\sigma = 1.8\,k_\mathrm{B}T$ is the standard deviation of the Gaussian-like thermal smearing function. Four histograms of spanning vectors were counted, one for each value of $c_i \in \{\frac{1}{3}, \frac{2}{3}, 1, \frac{4}{3}\}$. The histogram in Fig. 5 of the main text is an average of the four histograms, where each histogram is weighted according to the thermal smearing function.

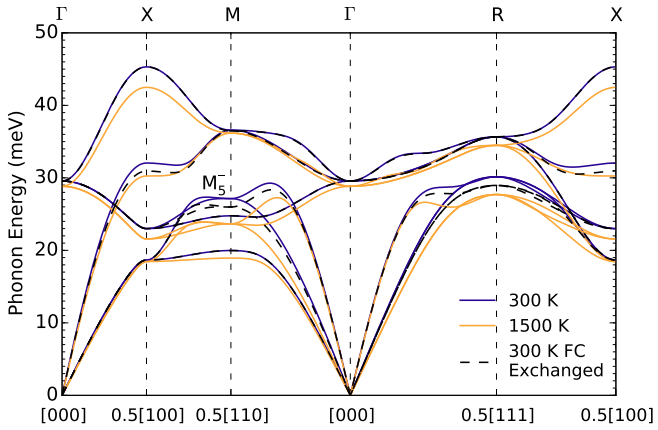

(a) Fe–Fe 2nn Longitudinal

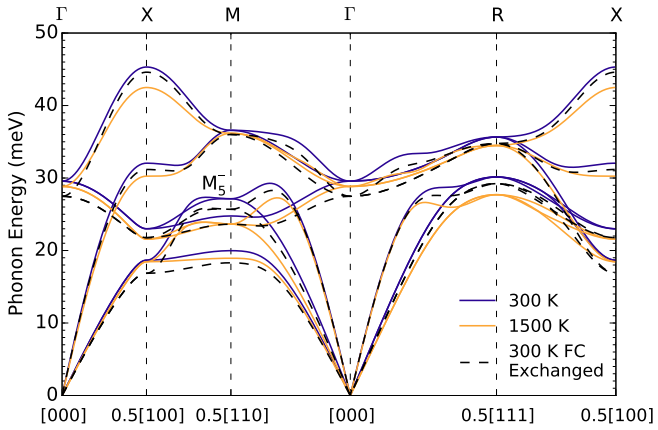

(b) Fe–Ti 1nn Transverse

FIG. 6. FeTi phonon dispersions calculated after individually exchanging the (a) Fe–Fe 2nn longitudinal and (b) Fe–Ti 1nn transverse force constants at 300 K with those at 1500 K.

[1] W. Sturhahn, Hyperfine Interact. **125**, 149 (2000).

[2] D. L. Abernathy, M. B. Stone, M. J. Loguillo, M. S. Lucas, O. Delaire, X. Tang, J. Y. Y. Lin, and B. Fultz, Rev. Sci. Instr. **83**, 015114 (2012).

[3] B. Fultz, T. Kelley, J. Lin, J. Lee, O. Delaire, M. Kresch, M. McKerns, and M. Aivazis, "Experimental inelastic neutron scattering: Introduction to DANSE," http://docs.danse.us/DrChops/ExperimentalInelasticNeutronScattering.pdf (2009).

[4] M. S. Lucas, J. A. Muñoz, O. Delaire, N. D. Markovskiy, M. B. Stone, D. L. Abernathy, I. Halevy, L. Mauger, J. B. Keith, M. L. Winterrose, Y. Xiao, M. Lerche, and B. Fultz, Phys. Rev. B **82**, 144306 (2010).

[5] J. A. Muñoz, M. S. Lucas, O. Delaire, M. L. Winterrose, L. Mauger, C. W. Li, A. O. Sheets, M. B. Stone, D. L. Abernathy, Y. Xiao, P. Chow, and B. Fultz, Phys. Rev. Lett. **107**, 115501 (2011).

[6] J. A. Muñoz, M. S. Lucas, L. Mauger, I. Halevy, J. Horwath, S. L. Semiatin, Y. Xiao, P. Chow, M. B. Stone, D. L. Abernathy, and B. Fultz, Phys. Rev. B **87**, 014301 (2013).

[7] J. A. Muñoz, *Electronic structure and phonon thermodynamics of iron alloys*, Ph.D. thesis, California Institute of Technology (2013).

[8] W. Kohn and L. J. Sham, Phys. Rev. **140**, A1133 (1965).

[9] G. Kresse and J. Furthmüller, Phys. Rev. B **54**, 11169 (1996).

[10] G. Kresse and J. Furthmüller, Comput. Mat. Sci. **6**, 15 (1996).

[11] J. P. Perdew, K. Burke, and M. Ernzerhof, Phys. Rev. Lett **77**, 3865 (1996).

[12] M. V. Nevitt, J. Appl. Phys. **31**, 155 (1960).

[13] H. J. Monkhorst and J. D. Pack, Phys. Rev. B **13**, 5188 (1976).

[14] K. Parlinski, Z-.Q. Li, and Y. Kawazoe, Phys. Rev. Lett. **78**, 4063 (1997).

[15] A. Togo, F. Oba, and I. Tanaka, Phys. Rev. B **78**, 134106 (2008).

[16] S. Baroni, S. de Gironcoli, A. Dal Corso, and P. Giannozzi, Rev. Mod. Phys. **73**, 515 (2001).

[17] P. Giannozzi *et al.*, J. Phys. Condens. Matter **21**, 395502 (2009).

[18] D. Vanderbilt, Phys. Rev. B **41**, 7892 (1990).

[19] S. Nosé, J. Chem. Phys. **81**, 511 (1984).

[20] P. V. C. Medeiros, S. Stafström, and J. Björk, Phys. Rev. B **89**, 041407 (2014).

[21] P. V. C. Medeiros, S. S. Tsirkin, S. Stafström, and J. Björk, Phys. Rev. B **91**, 041116 (2015).

[22] O. Hellman, I. A. Abrikosov, and S. I. Simak, Phys. Rev. B **84**, 180301 (2011).

[23] O. Hellman, P. Steneteg, I. A. Abrikosov, and S. I. Simak, Phys. Rev. B **87**, 104111 (2013).

[24] A. A. Maradudin and A. E. Fein, Phys. Rev. **128**, 2589 (1962).